Hyperfine interaction studies with ^{181}Ta and ^{111}Cd probes in the compound Ti_2Ag

2009 J. Phys.: Condens. Matter 21 095405

(http://iopscience.iop.org/0953-8984/21/9/095405)

J. Phys.: Condens. Matter **21** (2009) 095405 (7pp) doi:10.1088/0953-8984/21/9/095405

Hyperfine interaction studies with ^{181}Ta and ^{111}Cd probes in the compound Ti_2Ag

A Kulińska[1,2], P Wodniecki[1], B Wodniecka[1], H M Petrilli[3], L A Terrazos[4], M Uhrmacher[2] and K P Lieb[2]

[1] Institute of Nuclear Physics, Polish Academy of Sciences, Radzikowskiego 152, 31-342 Kraków, Poland
[2] II Physikalisches Institut, Georg-August-Universität Göttingen, Friedrich-Hund-Platz 1, D-37077 Göttingen, Germany
[3] Instituto di Fisica, Universidade de Sao Paulo, CP 66318, 05315-970, Sao Paulo, SP, Brazil
[4] Universidade Federal de Campina Grande, Centro de Educação e Saude, Cuite PB, 5817-000, Brazil

Received 7 October 2008, in final form 13 January 2009
Published 30 January 2009
Online at stacks.iop.org/JPhysCM/21/095405

Abstract
By using the time-differential perturbed angular correlation technique, the electric field gradients (EFG) at ^{181}Hf/^{181}Ta and ^{111}In/^{111}Cd probe sites in the $MoSi_2$-type compound Ti_2Ag have been measured as a function of temperature in the range from 24 to 1073 K. *Ab initio* EFG calculations have been performed within the framework of density functional theory using the full-potential augmented plane wave + local orbitals method as implemented in the WIEN2k package. These calculations allowed assignments of the probe lattice sites. For Ta, a single well-defined EFG with very weak temperature dependence was established and attributed to the [4(*e*)4*mm*] Ti site. For ^{111}Cd probes, two of the three measured EFGs are well defined and correlated with substitutional lattice sites, i.e. both the [4(*e*)4*mm*] Ti site and the [2(*a*)4/*mmm*] Ag site.

1. Introduction

Hyperfine interaction methods are among the most sensitive techniques for measuring magnetic and electric properties in the immediate neighborhood of probe atoms in elemental metal and semiconductor matrices or intermetallic compounds [1–3]. This well-known feature can be exploited to study, for example, lattice locations of impurity atoms as well as lattice dilations caused by them, and point defects trapped on them. However, there are only few intermetallic compounds for which first-principles calculations of the electric field gradients (EFGs) of probe atoms have been undertaken to check the assignments of impurity atoms to certain lattice sites (for examples see [4–7]). More often such assignments are based on heuristic (and sometimes invalid) arguments of lattice symmetry, atomic size and chemical valency.

The present work extends previous perturbed angular correlation (PAC) studies in the $MoSi_2$-type compounds Zr_2X and Hf_2X (X = Cu, Ag, Au, Pd) using ^{181}Hf/^{181}Ta probes [7, 8]. Here, we present measurements of the electric field gradients (EFGs) for the most common ^{181}Hf/^{181}Ta and ^{111}In/^{111}Cd PAC impurity probes in the Ti_2Ag phase, which is a member of the $C11_b$ group with a high c/a axis ratio and whose prototype is $MoSi_2$ [9, 10]. There are six atoms in the unit cell of the tetragonal $D^{17}_{4h}I4/mmm$ space group (see figure 1) and the EFG tensor is diagonal in the original crystal coordinate system. Both the Ti [4(*e*)4*mm*] and the Ag [2(*a*)4/*mmm*] lattice sites have an axial symmetry around the *c* axis. Contrary to the intermetallic Hf or Zr compounds doped with ^{181}Hf probes [4, 5] in Ti_2Ag, both the ^{111}In/^{111}Cd and ^{181}Hf/^{181}Ta probe species are different from the host constituents which complicates the interpretation of the measured perturbation spectra and the assignment to particular sites. Under these circumstances, EFG calculations are needed to solve the puzzle of how to interpret the measured quadrupole coupling constants. The EFGs have been calculated here *ab initio* within the Kohn–Sham scheme of the density functional theory using the augmented plane wave + local orbitals (APW + lo) method [11–13] as implemented in the WIEN2k package [14] and, indeed, by comparing the calculated EFGs with the experimentally measured values we have achieved unambiguous evidence for the lattice sites selected. Another motivation for the present work was to measure the temperature dependence of the EFGs, which in

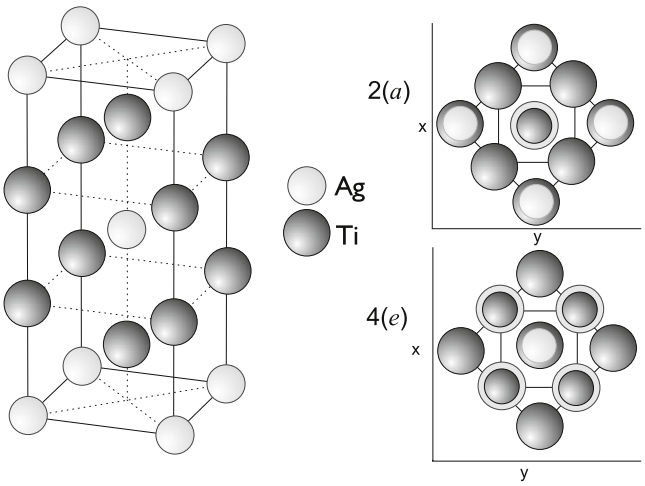

Figure 1. The crystal structure of the compound Ti_2Ag showing the $4(e)$ and $2(a)$ Ag sites.

intermetallic compounds of transition metals generally does not follow the $T^{3/2}$ rule [15], as shown for the above mentioned $MoSi_2$-type compounds [16].

2. Experimental details

A Ti_2Ag sample containing 33.6 at.% Ag was obtained by multiple arc melting under an argon atmosphere of the proper amounts of high purity Ti and Ag followed by 3 days of annealing at 800 °C. Powder x-ray diffraction established the $C11_b$ structure of the sample with a very small admixture of the TiAg phase (figure 2). Doping the sample with radioactive ^{111}In probes was done by irradiating at room temperature a 0.5 mm thick slice of the material with some 10^{12} radioactive ^{111}In ions at 400 keV by means of the Göttingen ion implanter IONAS [17]. After implantation the sample was evacuated in a quartz ampoule and annealed for 14 h at 700 °C and for another 2 h at 800 °C. This annealing procedure should allow us to remove the irradiation defects and diffuse the probe atoms to substitutional lattice sites. The ^{181}Hf activity was introduced by melting a very small amount of neutron-irradiated Hf metal with the Ti_2Ag material. This sample containing 32.65 at.% of Ag was then annealed in a vacuum for 2 days at 800 °C.

The PAC experiments were carried out with some four-detector apparatus described elsewhere [18] and covered the temperature range from 24 to 1073 K. Measurements below room temperature were accomplished by attaching the sample to a closed-cycle helium cryostat. The least squares fits of the perturbation factor for static electric hyperfine interactions [19] to the experimental data yielded the EFG tensors, each one characterized by its quadrupole frequency ν_Q and asymmetry parameter $\eta = (V_{xx} - V_{yy})/V_{zz}$. Broadenings of the EFGs were described by the widths δ of the Lorentzian ν_Q distributions. The values of the main EFG tensor component $|V_{zz}|$ were deduced from the measured quadrupole frequencies ν_Q by adopting the known quadrupole moment $Q = 2.36(5)b$ for the ^{181}Ta [20] isomeric state and $Q = 0.83(13)b$ for the ^{111}Cd [21] isomeric state. For both probe species and all the EFG fractions a linear temperature dependence was found and parameterized with the function $V_{zz}(T) = V_{zz}(0)[1 - \alpha T]$, α being a constant.

3. Experimental results

A PAC spectrum of Ti_2Ag taken at room temperature with ^{181}Hf/^{181}Ta probes is displayed in figure 3(a); its Fourier transform $P(\omega)$ shown in figure 3(b) exhibits a frequency triplet typical of a single, well-defined EFG. As expected from the crystalline $C11_b$ structure, the perturbation factor should indeed represent a single, axially symmetric EFG. At room temperature the fitted EFG has a principal component of $|V_{zz}| = 3.9 \times 10^{17}$ V cm^{-2} and a small, but non-vanishing, asymmetry parameter of $\eta = 0.13(2)$. The finite η value, which still increases at lower temperature (see figure 4), may possibly arise from lattice distortions around the oversized Hf probe impurity (see below). The width δ of the EFG distribution decreases slightly with increasing temperature, from 8% at 24 K to about 5% at 1000 K. We finally note

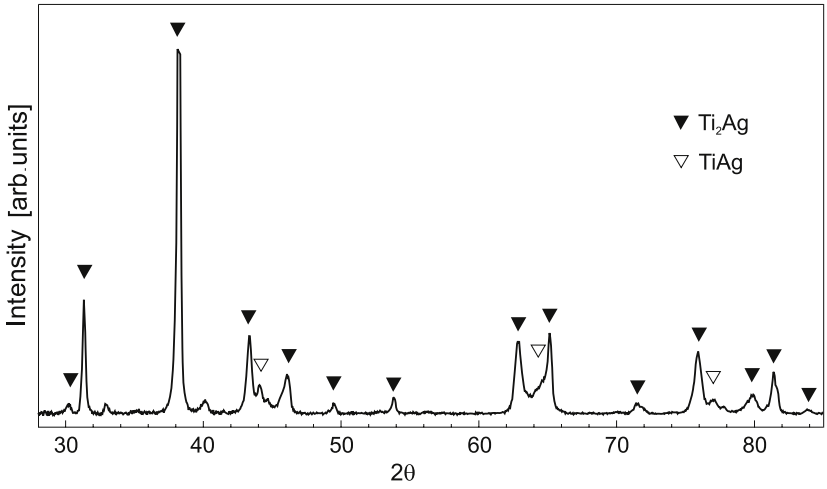

Figure 2. Powder x-ray diffraction pattern of the Ti_2Ag sample containing 33.6 at.% of Ag. Some traces of the TiAg phase are also evident.

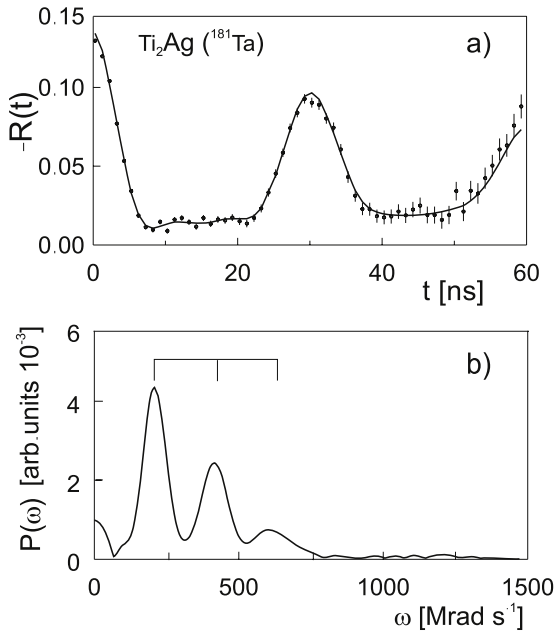

Figure 3. Room temperature PAC spectrum (a) and Fourier transform $P(\omega)$ (b) taken for ^{181}Ta probes.

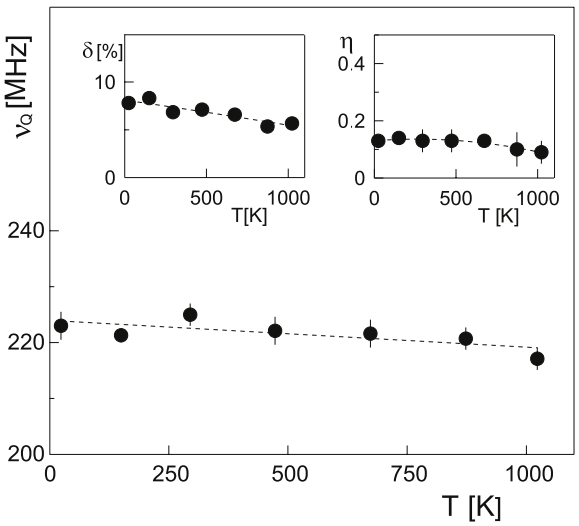

Figure 4. Temperature dependence of the quadrupole frequency ν_Q, relative width δ of the Lorentzian ν_Q-distribution, and asymmetry parameter η, measured with ^{181}Ta probes.

the very weak temperature dependence of the quadrupole frequency presented in figure 4. The dashed line represents a fit to the data with the slope parameter $\alpha = 0.20(2) \times 10^{-4}$ K^{-1}.

As shown in figures 5(a) and (b), the PAC pattern taken for ^{111}In/^{111}Cd probes in Ti_2Ag at room temperature is more complicated and exhibits several fractions, which possibly indicate various sites of the Cd probes in the lattice. Moreover, apart from the usually weak temperature dependence of the EFGs, the PAC spectra change their pattern as a function of the temperature, due to the changes in the fractions. Indeed, the temperature evolution of the Fourier transforms illustrated in figure 6 exhibits four fractions between 20 and 1073 K; two of them are present at all temperatures. One EFG fraction,

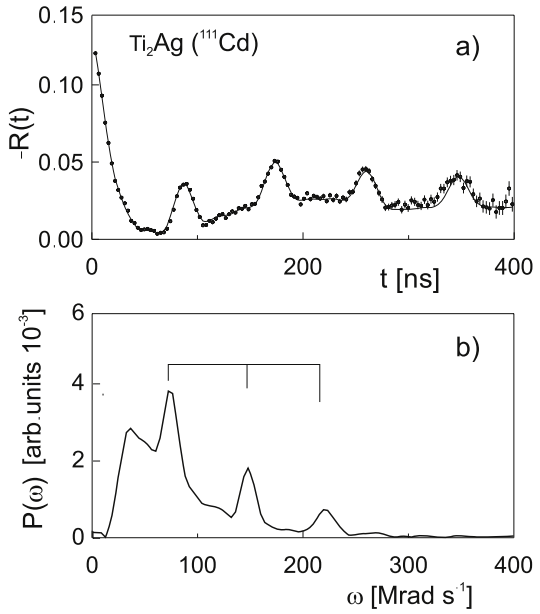

Figure 5. Room temperature PAC spectrum (a) and Fourier transform $P(\omega)$ (b) taken for the ^{111}Cd probes.

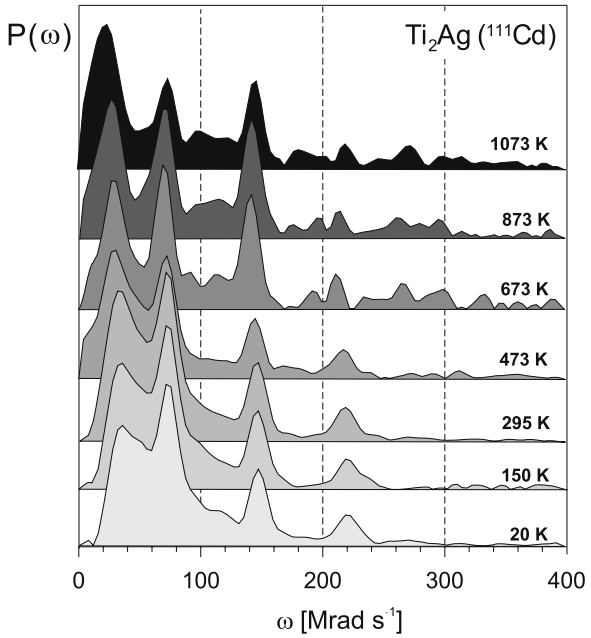

Figure 6. Temperature evolution of the PAC spectra measured with ^{111}Cd probes.

very well defined ($\delta < 1\%$), axially symmetric ($\eta = 0$) and corresponding to $|V_{zz}| = 3.8 \times 10^{17}$ V cm^{-2}, occurs with about 25% intensity. The temperature dependence of its EFG has a very small slope of $\alpha = 0.20(2) \times 10^{-4}$ K^{-1} as presented in figure 7. The second fraction has a lower EFG of $|V_{zz}| \approx 1.7 \times 10^{17}$ V cm^{-2}, a finite asymmetry parameter of $\eta \approx 0.3$, and a broader frequency width of $\delta \approx 20\%$ (growing with temperature); this fraction decreases with the temperature and in addition shows a pronounced decrease in its quadrupole frequency with a slope of $\alpha = 4.6(7) \times 10^{-4}$ K^{-1}. The third

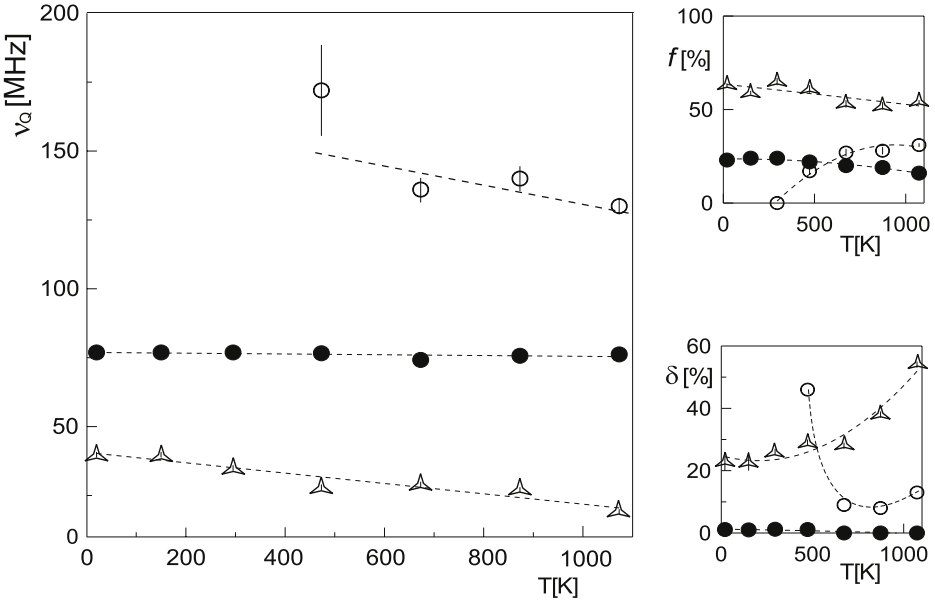

Figure 7. Temperature dependence of the quadrupole frequencies ν_Q, fractions f and relative widths δ of ν_Q-distributions, measured with ^{111}Cd probes.

Table 1. Room temperature quadrupole parameters for Cd and Ta probes in Ti_2Ag.

Probe	Fraction f (%)	ν_Q (MHz)	δ (%)	η	$\lvert V_{zz}\rvert$ (10^{17} V cm^{-2})	α (10^{-4} K^{-1})
^{181}Ta	100	223(2)	6(1)	0.13(2)	3.91(3)	0.2(1)
^{111}Cd	25(2)	77(1)	1.0(5)	0.0	3.83(5)	0.2(1)
	65(5)	35(1)	26(4)	0.24(5)	1.74(5)	4.6(7)
	10(2)	28(1)	6(2)	0.0	1.40(6)	

EFG, with $|V_{zz}| \approx 7.3 \times 10^{17}$ V cm^{-2} at room temperature and again $\eta = 0$, is identified only at temperatures above 300 K; its fraction grows strongly at 300–600 K and reaches about 30% at 1073 K. Initially its distribution width δ is rather high, but decreases to $\delta \approx 10\%$ at higher temperatures.

Below room temperature an additional small fraction of a small EFG, $|V_{zz}| = 1.40(6) \times 10^{17}$ V cm^{-2}, similar to that measured with Cd probes in the TiAg compound ($|V_{zz}| = 1.49(6) \times 10^{17}$ V cm^{-2}) by Wodniecki's group [22] was found and interpreted as due to the small TiAg phase admixture present in the $Ti_{66.4}Ag_{33.6}$ sample (see figure 2). No traces of the TiAg compound were observed in the Ta PAC spectra of the $Ti_{67.4}Ag_{32.6}$ sample. All the fitted values of the EFG parameters ν_Q, η, δ and $|V_{zz}|$ determined at room temperature for both probe species are collected in table 1.

4. Calculation and discussion

According to Darken and Gurry [25], impurity atoms can substitute for, in a defect-free manner, the host atoms in a metal matrix, whenever the electro-negativities and atomic sizes of the impurity and host atoms match each other. The corresponding Darken–Gurry diagram for In and Hf (mother) impurities and Ti and Ag constituents is shown in figure 8.

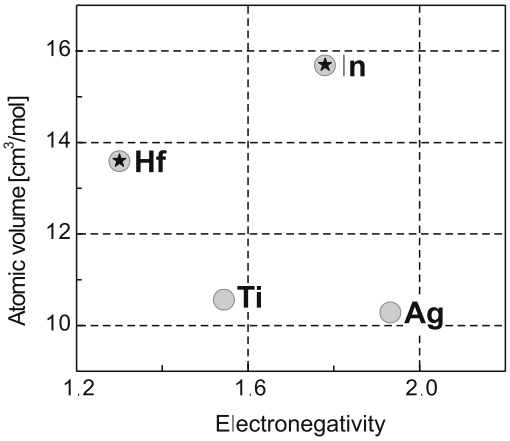

Figure 8. Comparison of atomic volumes and Pauling electro-negativities of the probe atoms (Hf, In) and compound constituent atoms (Ti, Ag) [23, 24].

Both impurities are oversized and also exhibit appreciable differences in electro-negativity. It was therefore *a priori* rather uncertain where to place the probe atoms. Evidently, In is about equally far away from Ti and Ag, while Hf is closer to Ti and consequently may substitute for Ti. For that reason, the ^{181}Hf/^{181}Ta probe used in the present study was treated as a dilute impurity in the Ti_2Ag compound, assuming that interstitial sites are unlikely and probe–defect configurations involving radiation defects are removed during the annealing process. For the ^{111}In/^{111}Cd probes, all possible defect-free dilute lattice sites were considered in the EFG calculations to be described now.

We have performed self-consistent electronic structure calculations using a $2 \times 2 \times 2$ super-cell with dimensions $2a$, $2a$ and $2c$, where a and c are the lattice parameters of the original unit cell. The lattice constants were fixed at the

Table 2. Comparison of the calculated EFGs (V_{zz}^{calc}) for substitutional ^{181}Ta and ^{111}Cd atoms in Ti_2Ag with the experimental values $|V_{zz}^{exp}|$ extrapolated to $T = 0$.

Site	$\lvert V_{zz}^{exp}(\text{Ta})\rvert$ (10^{17} V cm^{-2})	η^{exp}	V_{zz}^{calc}(Ta) (10^{17} V cm^{-2})	η^{calc}	$\lvert V_{zz}^{exp}(\text{Cd})\rvert$ (10^{17} V cm^{-2})	η^{exp}	V_{zz}^{calc}(Cd) (10^{17} V cm^{-2})	η^{calc}
Ti [4(*e*)4*mm*]	3.9(1)	0.13	+4.5	0.02	3.8(1)	0.0	+4.4	0.0
Ag [2(*a*)4/*mmm*]			−2.0	0.0	7.3(7)	0.0	−5.7	0.0
					2.0(1)	0.29		

experimental values of $a = 2.952$ Å and $c = 11.85$ Å [9, 10]. The Ta or Cd impurities replaced a Ti or Ag site near the center of this cell containing 48 atoms, which can be respectively reduced to 24 or 15 non-equivalent atoms, according to symmetry. In the WIEN2k implementation of the APW + lo method [11–14, 26, 27] the wavefunctions are expanded in spherical harmonics inside non-overlapping atomic spheres of radius *RMT*, and in plane waves in the remaining space of the unit cell (the interstitial region). For all elements we used 2.6 atomic units (au) as *RMT* values and 42 k-points in the irreducible wedge of the Brillouin zone. The maximum orbital angular momentum for the expansion of the wavefunction in spherical harmonics inside the spheres was taken to be $\ell_{max} = 10$. The plane wave expansion of the wavefunction in the interstitial region was made up to $K_{max} = 9.0/RMT = 3.46$ (au)$^{-1}$, and the charge density was Fourier expanded up to $G_{max} = 14$ Ryd$^{1/2}$. All these values were checked to yield numerically converging results. The Perdew–Burke–Ernzerhof generalized gradient approximation [28] was used as the exchange–correlation functional. Positional relaxation of the neighbors of the probe was included. The calculation for Ta in the Ti site was performed without any symmetry constraint (48 non-equivalent atoms), $K_{max} = 8.0/RMT = 3.08$ (au)$^{-1}$ and 25 k-points. The calculated EFGs correspond to zero temperature. Further details of the theoretical approach used here can be found in [11–14].

In table 2 the measured EFGs extrapolated to $T = 0$ are compared with the theoretical predictions. For both probe species the experimental and calculated values are in fair agreement. Regarding the typical accuracy of a few per cent in the calculated EFGs, reliable site assignments are indeed possible. The calculations demonstrate that the unique EFG present in the Ta PAC patterns correlates with the Ti [4*e*(4*mm*)] position as presumed from the Darken–Gurry diagram (figure 8). It can be concluded that all the Ta probes are found to be situated in the unique Ti lattice site, free of radiation defects. The measured small, but non-zero, value of the asymmetry parameter η and the EFG distribution width of a few per cent may be taken as evidence for lattice distortions around the oversized Ta probes. To investigate this point we have performed a calculation without any symmetry constraint in this case. Nevertheless, the η parameter remained very close to zero, even after full atomic relaxation around the Ta probe. On the other hand, the inclusion of full atomic relaxations changed the magnitude of the EFG by around 10% compared to the symmetry-constrained relaxations. Since the agreement between theory and experiment for V_{zz} in this case is rather good, the difference being less than 15%, and the predicted η value being close to zero, we conclude that Ta probe atoms indeed substitute Ti and the measured non-vanishing η value may be due to some other cause.

Table 3. Partial p–p and d–d contributions to the calculated EFGs in Ti_2Ag (in units of 10^{17} V cm^{-2}) of the Ta and Cd impurities substituting for Ag or Ti.

Site	V_{p-p}	V_{d-d}	Δn_p	Δn_d
		Impurity: Ta		
Ag	+3.92	−5.62	+0.0028	−0.15
Ti	+4.7	−0.42	+0.0071	−0.007
		Impurity: Cd		
Ag	−6.13	+0.34	−0.034	+0.0019
Ti	+4.89	−0.41	+0.025	−0.0041

Similarly, comparison of the measured and calculated EFGs for the Cd probes also allowed us to correlate the positions of the In mother atoms to the respective Ti_2Ag lattice sites. We conclude that at low temperature 25% of In/Cd are located in the regular [4*e*(4*mm*)] Ti position and that the site with the highest quadrupole frequency measured with Cd corresponds to the [2*a*(4/*mmm*)] Ag site. Above room temperature, the [2*a*(4/*mmm*)] Ag site also starts to become occupied and at 1000 K about half of the In/Cd probes are distributed between both regular lattice positions. The observed variation of the PAC fractions with the temperature, i.e. the deduced temperature dependence of the ^{111}In site populations, reminds us of the similar behavior of In impurities in the Laves phase $HfAl_2$ [29]. In this matrix a reversible switching of the ^{111}In probes between the Hf site below 300 K and the two Al sites at higher temperature has been found. In the spirit of the Darken–Gurry diagram it has been argued that the Hf site offers a larger volume to accommodate the oversized In atoms, while the Al sites offer better matching of the electronegativities. A recent EFG calculation by Belosevic-Cavor *et al* [30] in the frame of the APW + lo formalism indeed favored the Al site population. According to figure 8, there is evidently in Ti_2Ag a slightly better volume matching between In and Ti than between In and Ag.

To analyze the origin of the theoretical EFGs obtained here, we list in table 3 the partial p–p (V_{p-p}) and d–d (V_{d-d}) valence contributions to V_{zz} and the corresponding p and d charge anisotropies (Δn_p and Δn_d), using the usual notation [31]. In all the cases V_{p-p} is large and exceeds V_{d-d} by about one order of magnitude except for the Ta probe at the Ag site, where it is larger than the p contribution and with opposite sign. This is why V_{zz} is so small at this site. We also note that Δn_d is, in this case, much larger than at the other sites, which compensates the effect of the larger radial p–p integral

Table 4. Summary of the EFGs $|V_{zz}|$ measured for $^{181}\text{Hf} \rightarrow {}^{181}\text{Ta}$ probes in A_2B intermetallic compounds of $MoSi_2$ structure.

Compound	a (Å)	c (Å)	c/a	$\lvert V_{zz}\rvert^{\text{exp}}$ (10^{17} V cm^{-2})	α (10^{-4} K^{-1})
Hf_2Cu[a]	3.17	11.133	3.512	0.57(2)	Not measured
Zr_2Cu[b]	3.220	11.183	3.473	0.74	Not measured
Zr_2Au[c]	3.28	11.6	3.536	1.37(9)	Weakly rising
Hf_2Au[c]	3.231	11.606	3.592	1.91(9)	Weakly rising
Ti_2Ag[d]	2.952	11.85	4.014	3.91(3)	$\alpha = 0.2(1)$
Zr_2Ag[e]	3.246	12.004	3.698	4.36(4)	Weakly decreasing
Hf_2Ag[f]	3.10	11.53	3.72	5.05(5)	Very weak
Zr_2Pd[f]	3.306	10.894	3.295	5.10(7)	$\alpha = 5.2(2)$
Hf_2Pd[f]	3.251	11.061	3.402	5.34(3)	$\alpha = 4.9(2)$
Ti_2Rh[g]	3.078	9.882	3.211	5.89(2)	$\alpha = 0.36(2)$

[a] Reference [32]; [b] Reference [33]; [c] Reference [34];
[d] Present work; [e] Reference [35]; [f] Reference [7];
[g] Reference [36].

(mainly due to the large p wavefunction peak near the nuclear region) over the smaller radial d–d integral, leading to a net d contribution to V_{zz} that is larger than the p contribution.

Table 4 relates the now available EFG for ^{181}Ta probes in Ti_2Ag with those in other isostructural intermetallic compounds of the $C11_b$ structure [7, 8, 32, 36]. The smallest $|V_{zz}|$ values were measured at the 4(e) Hf site in Hf_2Cu [32] and at the Zr site in Zr_2Cu [33]. This low strength in quadrupole interaction has been explained as due to the unusually small contribution of the p orbital in this structure (being of the same order as the d term) [7, 37]. Table 4 also indicates that the $|V_{zz}|$ values at the 4(e) site in all the AB_2 compounds of the $C11_b$ structure grow when going from Cu through Au, Ag and Pd to $RhTi_2$. It seems that the electronic properties of the B-atom are at least equally important as the geometrical factors. The temperature dependences of most EFGs observed in these $MoSi_2$-type compounds are weak and sometimes $|V_{zz}|$ even rises with the temperature [34].

As pointed out above, the largest PAC fraction for In in Ti_2Ag, which amounts to 65% at low temperatures and decreases to 50% at 1000 K, has a strongly asymmetric EFG ($\eta = 0.24$) and a rather low quadrupole frequency ($\nu_Q = 35$ MHz). It may possibly be attributable to ^{111}In atoms on interstitial lattice site(s). As this PAC fraction appears rather stable over the full temperature range up to 1000 K, we assume that it does not originate from defect trapping. In many fcc and bcc metals single or multiple vacancy trapping on oversized indium during low temperature irradiation or implantation is known to create specific In-vacancy defect configurations, which, however, disappear upon annealing [1, 31]. Guided by these arguments, we disregard the possibility of such defect configurations in the present system, and consequently no interpretation has been found for this EFG fraction up to now.

5. Conclusions

The use of two radioactive impurity species (^{181}Hf, ^{111}In) as PAC probes in the intermetallic compound Ti_2Ag has allowed us, in combination with detailed calculations using the APW + lo method, to assign most measured EFGs to definite lattice sites. Although the agreement of the calculated and measured EFG values is less convincing than in our recent PAC study on ^{181}Hf/^{181}Ta probes in the Zr_4Al_3 and Hf_4Al_3 aluminides [5], these assignments in Ti_2Ag appear to be unambiguous. In view of the many PAC data available for ^{181}Ta in the isostructural intermetallic compounds of the $C11_b$ group listed in table 4, the present work may be particularly important for understanding all the other members of this class of compounds. Indeed, it would be worthwhile to perform systematic EFG calculations.

As in several cases studied before, the results for the ^{111}In/^{111}Cd impurity probes are less clear: various fractions of these impurity atoms end up on all the different possible lattice locations of both constituents, while another large fraction finds a thermally stable, but so far unidentified, site.

Acknowledgments

The authors acknowledge the help of D Purschke, Göttingen, during the ^{111}In ion implantations and the advice of Dr S Cottenier, Leuven, during the EFG calculations. This work has been funded by DAAD, DFG, FAPESP, Capes and Cnpq and used the computing facilities of LCCA-USP and CENAPAD.

References

[1] Schatz G and Weidinger A 1997 *Nukleare Festkörperphysik* (Stuttgart: Teubner) pp 78–114
Wichert Th, Achtziger N, Metzner H and Sielemann R 1992 *Hyperfine Interaction of Defects in Semiconductors* ed G Langouche (Amsterdam: Elsevier) p 77
[2] Lerf J and Butz T 1987 *Hyperfine Interact.* **36** 275
[3] Collins G and Zacate M 2001 *Hyperfine Interact.* **136/137** 541
[4] Wodniecki P, Kulińska A, Wodniecka B, Uhrmacher M and Lieb K P 2005 *Hyperfine Interact.* **158** 429
Wodniecki P, Kulińska A, Wodniecka B, Uhrmacher M and Lieb K P 2005 *Hyperfine Interact.* **158** 339 and references given there
[5] Wodniecki P, Kulińska A, Wodniecka B, Cottenier S, Petrilli H M, Uhrmacher M and Lieb K P 2007 *Europhys. Lett.* **77** 43001
[6] Torumba D, Vanhoof V, Rots M and Cottenier S 2006 *Phys. Rev.* B **74** 14409
Torumba D, Novak P and Cottenier S 2008 *Phys. Rev.* B **77** 155101
[7] Terrazos L A, Petrilli H M, Marszalek M, Saitovich H, Silva P R J, Blaha P and Schwarz K 2002 *Solid State Commun.* **121** 525
[8] Wodniecka B, Marszałek M, Wodniecki P, Saitovitch H, da Silva P R J and Hrynkiewicz A Z 1995 *J. Alloys Compounds* **219** 132
Wodniecki P, Wodniecka B, Marszałek M and Hrynkiewicz A Z 1996 *Z. Naturf.* a **51** 437
[9] Eremenko V N, Buyanov Yu I and Panchenko N M 1970 The liquidus surface of the system titanium–copper–silver *Poroshkovaya Metall. Kiev.* **9** 301
Eremenko V N, Buyanov Yu I and Panchenko N M 1970 *Sov. Powder Metall. Met. Ceram.* **10** 301 (Engl. Transl.)
[10] Nevitt M N and Downey J W 1962 *Trans. AIME* **224** 195
Schubert K, Meissner H G, Raman A and Rossteutscher W 1964 *Naturwissenschaften* **51** 287
Raman A and Schubert K 1964 *Z. Metallk.* **55** 798

See also Eckerlin P and Kandler H 1971 *Structure Data of Elements and Intermetallic Phases* (*Landolt–Börnstein—Group III Condensed Matter* vol 6) (Heidelberg: Springer) p 1615
[11] Madsen G K H, Blaha P, Schwarz K, Sjöstedt E and Nordström L 2001 *Phys. Rev.* B **64** 195134
[12] Cottenier S 2002 *Density Functional Theory and the Family of (L)APW-Methods: A Step-By-Step Introduction* Instituut voor Kern-en Stralingsfysica, KU Leuven, Belgium, available from http://fys.kuleuven.be/iks/nvsf/publications/DFT_and_LAPW.pdf ISBN 90-807215-1-4
[13] Sjöstedt E, Nordström L and Singh D J 2000 *Solid State Commun.* **114** 15
[14] Blaha P, Schwarz K, Madsen G, Kvasnicka D and Luitz J 1999 *WIEN2k, An Augmented Plane Wave + Local Orbitals Program for Calculating Crystal Properties* K Schwarz, Technische Universität Wien, Austria ISBN 3-9501031-1-2
[15] Christiansen J, Heubes P, Keitel R, Klinger W, Loeffler W, Sandner W and Witthuhn W 1976 *Z. Phys.* B **24** 177
[16] Verma H C and Rao G N 1983 *Hyperfine Interact.* **15/16** 207
[17] Uhrmacher M, Pampus K, Bergmeister F J, Purschke D and Lieb K P 1985 *Nucl. Instrum. Methods* B **9** 234
[18] Lupascu D, Habenicht S, Lieb K P, Neubauer M, Uhrmacher M, Wenzel Th and ISOLDE-Collaboration 1996 *Phys. Rev.* B **54** 871
[19] Frauenfelder H and Steffen R M 1963 *Perturbed Angular Correlations* ed K Karlsson, E Matthias and K Siegbahn (Amsterdam: North-Holland)
[20] Butz T and Lerf A 1983 *Phys. Lett.* A **97** 217
[21] Herzog P, Freitag K, Reuschenbach M and Walitzki H 1980 *Z. Phys.* A **294** 13
[22] Wodniecki P, Kulińska A and Wodniecka B 2006 unpublished
[23] Moses A J (ed) 1978 *The Practicing Scientist's Handbook* (London: Van Nostrand-Reinhold)
[24] Allred A 1961 *J. Inorg. Nucl. Chem.* **17** 215
[25] Darken L S and Gurry R W 1953 *Physical Chemistry of Metals* (New York: McGraw-Hill)
[26] Petrilli H M, Blöchl P E, Blaha P and Schwarz K 1998 *Phys. Rev.* B **57** 14690
[27] Errico L A, Fabricius G, Rentería M, de la Presa P and Forker M 2002 *Phys. Rev. Lett.* **89** 055503
[28] Perdew J P, Burke K and Ernzerhof M 1996 *Phys. Rev. Lett.* **77** 3865
[29] Wodniecki P, Wodniecka B, Kulińska A, Uhrmacher M and Lieb K P 2001 *Phys. Lett.* A **288** 227
Wodniecki P, Wodniecka B, Kulińska A, Uhrmacher M and Lieb K P 2002 *J. Alloys Compounds* **335** 20
[30] Belosevic-Cavor J, Koteski V, Cekić B and Umićević M 2007 *Comput. Mater. Sci.* **41** 164
[31] Blaha P, Schwarz K and Dederichs P H 1988 *Phys. Rev.* B **37** 2792
[32] Damonte L C, Mendoza-Zélis L A and López-Garcia A R 1989 *Phys. Rev.* B **39** 12492
[33] Mendoza-Zélis L A, Damonte L C, Bibiloni A G, Desimoni J and López-Garcia A R 1986 *Phys. Rev.* B **34** 2982
[34] Marszałek M, Saitovitch H and da Silva P R J 1994 *Annual Report* The H Niewodniczański Institute of Physics, Cracow, Poland p 28
[35] Wodniecki P, Wodniecka B and Kulińska A 2003 *Phys. Status Solidi* b **236** 565
[36] Wodniecki P, Kulińska A and Wodniecka B 2009 *Hyperfine Interact.* **177** 97
[37] Petrilli H M and Frota-Pessôa S 1993 *Phys. Rev.* B **48** 7148